Atmos. Meas. Tech. Discuss., 8, 9823–9851, 2015
www.atmos-meas-tech-discuss.net/8/9823/2015/
doi:10.5194/amtd-8-9823-2015

Atmospheric Measurement Techniques Discussions
Open Access

Ionosonde measurements in Bayesian statistical ionospheric tomography with incoherent scatter radar validation

J. Norberg[1], I. I. Virtanen[2], L. Roininen[2,3], J. Vierinen[4], M. Orispää[2], K. Kauristie[1], and M. S. Lehtinen[2]

[1]Finnish Meteorological Institute, Helsinki, Finland
[2]Sodankylä Geophysical Observatory, University of Oulu, Sodankylä, Finland
[3]Tallinn University of Technology, Tallinn, Estonia
[4]Massachusetts Institute of Technology, Westford, Massachusetts, USA

Received: 26 August 2015 – Accepted: 27 August 2015 – Published: 21 September 2015

Correspondence to: J. Norberg (johannes.norberg@fmi.fi)

Published by Copernicus Publications on behalf of the European Geosciences Union.

Abstract

We validate two-dimensional ionospheric tomography reconstructions against EISCAT incoherent scatter radar measurements. Our tomography method is based on Bayesian statistical inversion with prior distribution given by its mean and covariance. We employ ionosonde measurements for the choice of the prior mean and covariance parameters, and use the Gaussian Markov random fields as a sparse matrix approximation for the numerical computations. This results in a computationally efficient and statistically clear inversion algorithm for tomography.

We demonstrate how this method works with simultaneous beacon satellite and ionosonde measurements obtained in northern Scandinavia. The performance is compared with results obtained with a zero mean prior and with the prior mean taken from the International Reference Ionosphere 2007 model. In validating the results, we use EISCAT UHF incoherent scatter radar measurements as the ground truth for the ionization profile shape.

We find that ionosonde measurements improve the reconstruction by adding accurate information about the absolute value and the height distribution of electron density, and outperforms the alternative prior information sources. With an ionosonde at continuous disposal, the presented method enhances stand-alone near real-time ionospheric tomography for the given conditions significantly.

1 Introduction

In ionospheric satellite tomography the electron density distribution of the ionosphere is reconstructed from ground-based measurements of satellite-transmitted radio signals. The use of tomographic methods for ionospheric research was first suggested by Austen et al. (1988). Bust and Mitchell (2008) provide a good overview on the development of the topic.

AMTD
8, 9823–9851, 2015

Mathematically ionospheric tomography is an ill-posed inverse problem and cannot be solved without some additional stabilizing or regularizing information. In ionospheric tomography the additional information is often incorporated with the use of iterative reconstruction algorithms such as algebraic reconstruction technique with a strong initial model for the ionosphere (Andreeva, 1990). Bayesian statistical inversion was applied to ionospheric tomography first by Markkanen et al. (1995). The Bayesian approach provides an interpretable approach for the stabilization as the additional information is given as a prior probability distribution of unknown parameters. However, in the work of Markkanen et al. (1995), the prior distribution is not defined by its covariance, but by an assumption of smoothness resulting from the limiting of the differences of neighboring pixels. This is an often valid assumption, but the relation between the prior parameters and the physical quantities is not clear. Recently, Norberg et al. (2015) have described a method in which the prior can be built in a computationally efficient way as a probability distribution with a known covariance structure. The prior is parametrized with physical units and can be understood as a probability distribution for realizations of the ionosphere.

Regardless of the tomographic algorithm in use, the information provided by satellite to ground measurements is poor in the vertical direction. This is due to the limited measurement geometry, namely the lack of horizontal signal paths. Consequently, the peak altitude and the vertical gradient of the reconstructed ionosphere will be determined mostly by the regularizing prior assumptions that are built-in to the employed tomography algorithm. In this study we employ the ionosonde measurements to give these assumptions for the vertical profile.

An ionosonde is a radar used to investigate the ionosphere. An ionosonde transmits electromagnetic frequency pulses, sweeping through the high frequency (HF) range, and receives the signals reflected from an altitude where the radar frequency matches a critical frequency. For ordinary mode polarization the critical frequency is the plasma frequency of the local electron density. Because refractive index along the signal path differs significantly from that of vacuum, conversion of signal travel time into reflection

AMTD
8, 9823–9851, 2015

height is not trivial, but the electron density profile along the path needs to be taken into account. The reflections and the travel times at multiple frequencies can be used to estimate an electron density profile of the ionosphere. Because the ionosonde relies on reflection, it can directly measure only the bottom side of the ionospheric altitude profile up to the peak of the electron density profile. Also, it is not very effective for observing local minima, e.g., the valley region between the E- and F-regions of the ionosphere. Ionosonde measurements provide recurrent and accurate, but geographically localized information of the ionospheric electron density profile. In mesoscale tomographic analysis, it is often the best information available, even if the analyzed region is somewhat displaced from the ionosonde site.

Inclusion of ionosonde measurements in ionospheric tomography has been studied by Kersley et al. (1993), where ionosonde measurements were used to form the background profile for an iterative reconstruction algorithm. The study had mixed results on the impact of ionosonde measurements inclusion. They also observed up to 70 % differences between the ionosonde and incoherent scatter radar derived electron density profiles. More recently Chartier et al. (2012) used ionosonde measurements to set vertical basis functions for the inversion, as well as using them as local measurements of peak density and bottom-side profile gradients. The inclusion improved the tomographic results significantly, but the sensitivity to ionosonde measurement bias was also underlined.

In this article we continue the work presented in Norberg et al. (2015) and include the ionosonde measurements in the Bayesian statistical inversion approach for ionospheric tomography. For comparison, we analyze the data also with the prior mean taken from the International Reference Ionosphere (IRI) model, and with a zero-mean prior. We construct the prior mean electron density profile for the entire ionospheric tomography domain according to the chosen information source. This assumption is then controlled with the prior covariance, as it states how strictly the reconstruction should follow the prior mean. As the prior distribution is parametrized with physical units, the method provides clear understanding on information used for the tomographic reconstruction.

AMTD
8, 9823–9851, 2015

Hence the approach makes the inversion possible with less ad hoc adjustment. This is a very important aspect for achieving reliable operational near real-time tomography results.

The approach is applied to Scandinavian sector with tomographic measurements from the TomoScand receiver chain (Vierinen et al., 2014) and ionosonde data from the European Incoherent Scatter Scientific Association (EISCAT) dynasonde in Tromsø, Norway. The IRI model used for the comparison is the International Reference Ionosphere 2007 (IRI-2007) (Bilitza and Reinisch, 2008). We validate the results with EISCAT ultra high frequency (UHF) incoherent scatter radar measurements carried out on 20 and 21 November 2014, and 11 and 14 March 2015 in Tromsø. Electron density profiles measured with the EISCAT UHF are routinely calibrated by means of comparing F-region peak electron density estimates from the UHF and the dynasonde. Thus, when the ionosonde-based prior is used, F-region peak densities above the Tromsø site are taken from the same instrument in both the tomography prior mean and the UHF results. Our tomography measurements and the ground truth UHF measurements are thus not completely independent. However, we anticipate that this is not a very serious problem, because the calibration does not affect the UHF density profile shape, but only its absolute values, and because we have not calibrated individual profiles, but same scaling is used for a longer period of time. Especially, the actual validation measurements with beam steered far away from zenith are never used for calibration.

2 Methodology

The dual-frequency signal transmitted from low Earth orbit (LEO) satellites consists frequencies of 150 and 400 MHz. The ionospheric refraction causes a phase shift to propagating electromagnetic waves. This phase shift is proportional to density of elec-

AMTD
8, 9823–9851, 2015

trons along the signal path (Davies, 1990), and can be modelled as

$$m_t = \gamma + \int_{L_t} N_e(z)\mathrm{d}z + \varepsilon_t, \quad (1)$$

where m_t is the measured relative total electron content at time t and ε_t the corresponding measurement error. $N_e(z)$ is the two-dimensional continuous field of electron densities with coordinates $z := (z_1, z_2) \in \mathbb{R}^2$. The integral is defined over the measurement signal path L_t. The receiver-satellite specific constant γ is due to the unknown amount of electron content when the satellite is first observed.

For practical computations, we discretize Eq. (1) for all measurements $t = 1, \ldots, n_m$. Then the discretized measurement model for the ionospheric tomography is given as

$$\boldsymbol{M} = \mathbf{A}\boldsymbol{X} + \boldsymbol{E}. \quad (2)$$

The measurement vector is $\boldsymbol{M} \in \mathbb{R}^{n_m}$. Theory matrix $\mathbf{A} \in \mathbb{R}^{n_m \times n_x}$ gives the measurement geometry between the satellite measurement points and receiver locations. The vector of unknown parameters $\boldsymbol{X} \in \mathbb{R}^{n_x}$ includes both electron densities and the 2π-ambiguity constants γ. The measurement error vector is $\boldsymbol{E} \in \mathbb{R}^{n_m}$. The number of measurements is given as n_m and the number of unknown parameters as n_x.

Let us denote by $\boldsymbol{x}$ and $\boldsymbol{m}$ the realizations of the random variables $\boldsymbol{X}$ and $\boldsymbol{M}$, respectively. We can then write the likelihood function for unknown parameters, given the measurements as

$$\mathcal{L}(\boldsymbol{x}|\boldsymbol{m}) = D_E(\mathbf{A}\boldsymbol{x} - \boldsymbol{m}), \quad (3)$$

where D_E is the probability density function of measurement errors. From here on we assume that $\boldsymbol{E} \sim \mathcal{N}(\mathbf{0}, \boldsymbol{\Sigma}_E)$, i.e. the measurement errors follow a multivariate normal distribution with zero mean and covariance $\boldsymbol{\Sigma}_E \in \mathbb{R}^{(n_m)\times(n_m)}$.

As the ionospheric tomography is an ill-posed problem, the maximum likelihood estimate for Eq. (3) cannot be solved without including some additional information regarding the unknown parameters. Here we use Bayesian statistical inversion (Markkanen

AMTD
8, 9823–9851, 2015

et al., 1995; Kaipio and Somersalo, 2005) to give this information as a prior distribution. We assume that the unknown $\mathbf{X}$ follows a multivariate normal distribution $\mathbf{X} \sim \mathcal{N}(\boldsymbol{\mu}, \boldsymbol{\Sigma}_{\mathrm{pr}})$, where vector $\boldsymbol{\mu} \in \mathbb{R}^{n_x}$ is the mean value and the matrix $\boldsymbol{\Sigma}_{\mathrm{pr}} \in \mathbb{R}^{(n_x)\times(n_x)}$ the covariance. We denote the prior probability density function with $D_{\mathrm{pr}}(\boldsymbol{x})$. Following the Bayes' theorem, we then obtain the *posterior distribution* for $\boldsymbol{X}$ as

$$D_{\mathrm{post}}(\boldsymbol{x}|\boldsymbol{m}) = \frac{D_E(\mathbf{A}\boldsymbol{x} - \boldsymbol{m})D_{\mathrm{pr}}(\boldsymbol{x})}{\int_{\mathbb{R}^{n_x}} D_E(\mathbf{A}\boldsymbol{x} - \boldsymbol{m})D_{\mathrm{pr}}(\boldsymbol{x})\mathrm{d}\boldsymbol{x}}, \tag{4}$$

where the denominator is a normalization constant and we can write

$$D_{\mathrm{post}}(\boldsymbol{x}|\boldsymbol{m}) \propto D_E(\mathbf{A}\boldsymbol{x} - \boldsymbol{m})D_{\mathrm{pr}}(\boldsymbol{x}). \tag{5}$$

From the posterior distribution we can then derive the most probable value for the unknown parameters based on the prior distribution and observed measurements, namely, the *maximum a posteriori estimator* (MAP)

$$\boldsymbol{x}_{\mathrm{MAP}} = \boldsymbol{\Sigma}_{\mathrm{post}} \left(\mathbf{A}^{\mathrm{T}} \boldsymbol{\Sigma}_E^{-1} \boldsymbol{m} + \boldsymbol{\Sigma}_{\mathrm{pr}}^{-1} \boldsymbol{\mu} \right), \tag{6}$$

where

$$\boldsymbol{\Sigma}_{\mathrm{post}} = \left(\mathbf{A}^{\mathrm{T}} \boldsymbol{\Sigma}_E^{-1} \mathbf{A} + \boldsymbol{\Sigma}_{\mathrm{pr}}^{-1} \right)^{-1} \tag{7}$$

is called *posterior covariance*.

As we assume that the unknown parameters follow multivariate normal distribution, the prior density function $D_{\mathrm{pr}}(\boldsymbol{x})$ is defined with its mean and covariance. In Bayesian statistical approach for ionospheric tomography, the prior mean can be understood as the most probable state of the ionosphere before the actual satellite measurements. With the covariance we can express how reliable the information of prior mean is and

AMTD
8, 9823–9851, 2015

how correlated the ionospheric electron densities are. Actual values of these parameters should be based on all information we have in our disposal, i.e. on other measurements, models, statistical data and the physics of ionosphere. In the performed experiments, we use three different schemes to compose the prior: IRI-2007 ionospheric model, zero mean, and most importantly, the ionosonde measurements. The prior covariance is given as a squared exponential, i.e. as a Gaussian-shaped function that is defined with its amplitude (variance scaling factor) and correlation length. The correlation length is given separately for horizontal and vertical directions and is defined here as the distance where the covariance drops to 10 % of variance.

It is very natural to represent the prior information as a probability distribution. However, for the MAP estimator Eq. (6) only the precision matrix $\mathbf{\Sigma}_{\text{pr}}^{-1}$, i.e. the inverse of the prior covariance, is required besides the prior mean. In Norberg et al. (2015) it is shown how the precision matrix of a known covariance can be constructed with a sparse matrix representation with Gaussian Markov random fields. The approach provides us with the interpretation of a probability distribution, yet it keeps the approach computationally feasible, in comparison to operating with full covariance matrices.

Unfortunately, the linear system allows also negative values in the solution. If negative values are found we add them as new measurements into the linear system. We then set these new measurements to zero with a small variance (10^{-20}) and solve the system again.

3 Experiments

Two EISCAT UHF incoherent scatter radar measurement campaigns were performed in November 2014 and March 2015. Three daytime and one night time COSMOS satellite overflights, suitable for two-dimensional tomography, were measured with TomoScand receivers starting approximately at 20 November 2014 12:50, 3 November 2015 13:50, 14 March 2015 13:20 and 21 November 2014 02:50 UTC. The altitude of COSMOS satellites is approximately 1000 km and the duration of measurements from an over-

AMTD
8, 9823–9851, 2015

flight roughly 10 min. For the ionosonde prior mean the NeXtYZ (Zabotin et al., 2006) analyzed EISCAT dynasonde results from Tromsø[1] were collected. The ionosonde electron density profiles that were measured during each satellite overflight were averaged together to form one profile. We denote the resulting profile with μ_{NeXtYZ}. The NeXtYZ provides also a modeled profile for the top-side ionosphere, but to gain better control over the prior, we here give the top-side as an exponential profile. The complete altitude profile for the prior mean based on ionosonde measurement can be written as

$$\mu_{\text{ionosonde}}(z) = \begin{cases} \mu_{\text{NeXtYZ}}(z_{\text{peak}}) \exp\left(-\frac{z - z_{\text{peak}}}{s}\right), & z_{\text{peak}} < z \le z_{\text{max}} \\ \mu_{\text{NeXtYZ}}(z), & 0 \le z \le z_{\text{peak}}, \end{cases} \tag{8}$$

where z is the altitude with the maximum $z_{\text{max}} = 1000$ (km) and $z_{\text{peak}} = \underset{z}{\text{argmax}}(\mu_{\text{NeXtYZ}}(z))$, i.e. the altitude of the maximum electron density. The parameter s defines how rapidly the electron density decreases at the higher altitudes.

The IRI-2007 electron density profiles[2] were taken for the reconstruction times with longitude parameter 26°. With the IRI-2007 we obtain a two-dimensional profile with latitudinal variation for the complete domain where the ionospheric tomography takes place.

To validate the resulting tomographic reconstructions, for each satellite overflight, the EISCAT UHF was set to perform a scan of four measurements along the corresponding satellite track. As explained in Sect. 1, the UHF data were calibrated against the EISCAT Tromsø dynasonde. The calibration data were taken from periods when the radar was not scanning and the ionosphere was reasonably stable. Each few hours long continuous radar run was calibrated separately.

In the following three subsections we compare the EISCAT UHF measurements to corresponding electron density profiles from the obtained tomographic reconstructions.

[1]These are available from the EISCAT Dynasonde Database (http://dynserv.eiscat.uit.no/DD/Iono_form.php).

[2]Available from the IRI-2007 website (http://omniweb.gsfc.nasa.gov/vitmo/iri_vitmo.html).

AMTD
8, 9823–9851, 2015

With the Overflight I the reconstruction was made multiple times to choose the measurement domain and prior parameters other than the prior mean. Based on these trials the measurements used for the tomography were limited between the latitudes of 55° and 75°, and the elevation angles over 20°. The prior standard deviation (SD) is given as a Chapman function for the vertical profile, with approximately the same peak altitude than the prior mean, and the maximum electron density approximately 40 % of the corresponding NeXtYZ maximum. The Chapman profile was modified to have different scale heights for above and below the maximum. The chosen values used here are 200 and 60 km correspondingly. In vertical direction the prior correlation length was chosen to be 200 km and in the horizontal 2°. The s parameter for the upper profile of the prior was chosen to be 140 km. This results as a slightly steeper gradient for the top-side ionosphere than provided by NeXtYZ. With the zero mean prior we use the same prior standard deviation as with the ionosonde case but, to allow larger changes in electron density, the maximum is set to 80 % of the NeXtYZ maximum. The resolution for the domain is 200 × 200, resulting in pixel size of 5 km × 0.1°. After calibrating the parameters with the Overflight I, for the Overflights II and III the parameter values are adjusted only according to corresponding ionosonde measurements without additional tuning. For the Overflight IV the ionosonde profiles differ significantly from the previous ones. Hence also the prior standard deviation shape is adjusted to correspond these conditions.

In each of the following cases we first visualize the general measurement setup on a map in Figs. 1, 3, 5 and 7. The results are presented in Figs. 2, 4, 6 and 8, first as two-dimensional altitude-latitude reconstructions of electron densities, i.e. the MAP estimates where the ionosonde prior is used. On top of the reconstruction the EISCAT UHF scans are shown with white paths. We then compare the prior and posteriori distribution parameters to corresponding EISCAT UHF scan locations by assuming longitudinally uniform ionosphere. The ionosonde prior means are plotted with solid green lines and the 95 % prior credible intervals (Ionosonde prior mean ±2 × prior SD) with dashed green lines. The profiles taken from the reconstruction with ionosonde

AMTD
8, 9823–9851, 2015

prior are plotted with solid black lines (MAP ionosonde) and the corresponding 95 % posterior credible intervals with dashed black lines (MAP ionosonde ±2 × posterior SD). The electron density profiles obtained with EISCAT UHF scans are plotted with red. The blue dashed line is a profile taken from the reconstruction where the prior is based on IRI-2007 profile (MAP IRI) and the cyan dashed line from the reconstruction with zero mean prior (MAP ZERO). In Tables 1–4 the relative mean errors for profile peak electron densities and the mean errors for peak altitudes are given. In addition to the profile comparisons, we show the relative phase difference measurements used for the inversion for each station, as well as the corresponding measurements predicted from the reconstruction obtained with ionosonde prior.

3.1 Overflight I

The COSMOS 2463 overflight (Fig. 1) starts at 20 November 2014 12:50 UTC. The direction of the satellite track is from north to south. The relative phase difference curves in the top right panel of Fig. 2 indicate smooth ionosphere, with some local structures visible in the Tromsø station curve. The ionosonde measurements used for the prior are from 12:54, 12:56, 12:58 and 13:00 UTC. In Fig. 2, the obtained tomographic reconstruction is shown in the top left panel. On top of the reconstruction are plotted the four EISCAT UHF measurements performed at (1) 12:53:00–12:54:10, (2) 12:55:03–12:56:03, (3) 12:56:20–12:57:20, and, (4) 12:57:35–12:58:35 UTC. The latitude–longitude directions of the measurement can be seen in Fig. 1. Hourly averaged Kp and F10.7 indices at 13:00 UTC were 1.3 and 164.1, respectively. The magnetic local time is approximately UTC + 2.5 h.

The profile comparisons 1–4 in Fig. 2 show that the southward increment of electron density is captured by all three reconstructions. In the profiles based on the IRI-2007 and zero mean prior reconstructions the maximum electron density is significantly lower than in the EISCAT UHF profiles and shape of the profiles clearly disagrees with the UHF measurements in comparisons 1 and 2. With IRI-2007 the peak altitude is underestimated in all of the profiles. The ionosonde prior show a good agreement

AMTD
8, 9823–9851, 2015

between shapes of the corresponding profiles. Although the satellite rises almost to zenith above Tromsø, F-region peak density estimates from the ionosonde are about 30 % higher than the calibrated UHF measurements. However, the prior standard deviation enables large enough changes to capture the correct level in the MAP estimate. With the ionosonde prior the most glaring difference between the UHF and tomographic profiles is in the altitude of the peak electron densities.

3.2 Overflight II

The COSMOS 2407 overflight starts approximately at 3 November 2015 13:50 UTC (Fig. 3). The direction of the satellite track is from north to south. The relative phase difference curves in Fig. 4 indicate a smooth ionosphere. Based on the ionosonde measurements collected at 13:54, 13:56, 13:58 and 14:00 UTC the electron density level is expected to be lower than in Overflight I. The new prior profiles for this overflight are shown in the lower four panels of Fig. 4. Besides the altitude profiles for prior mean and standard deviation, the other parameters remain unchanged. In the top left panel of Fig. 4 the reconstruction and the EISCAT UHF measurement projections from (1) 13:54:28–13:55:28, (2) 13:55:50–13:56:50, (3) 13:57:11–13:58:11 and (4) 13:58:26–13:59:30 UTC are shown. Hourly averaged Kp and f10.7 indices at 14:00 UTC were 2.3 and 129.9, respectively. The magnetic local time is approximately UTC + 2.5 h.

The IRI-based profiles have very good agreement with the maximum densities of EISCAT scans. However the peak altitude is underestimated. The profiles taken from the reconstruction with zero mean prior clearly disagree with the UHF measurement, in terms of both profile shape and peak electron density.

With the ionosonde-based prior, in Profile comparison 1 the prior mean and the closest UHF measurement are very similar and also the tomographic reconstruction is almost unchanged from the prior profile. Again, the electron density slightly increases southwards, which is well captured in the reconstruction. Both, the peak density and altitude are very close to each other between the reconstruction and UHF profiles.

AMTD
8, 9823–9851, 2015

3.3 Overflight III

The COSMOS 2407 overflight starting at 14 March 2015 13:20 UTC (Fig. 5). The direction of the satellite track is from north to south. The ionosonde measurements used for the prior were collected at 13:26, 13:28, 13:30 and 13:32 UTC. The reconstruction and the EISCAT UHF measurement directions at (1) 13:27:45–13:28:45, (2) 13:29:01–13:30:02, (3) 13:30:20–13:31:21 and (4) 13:31:35–13:32:35 UTC are shown in the top left panel of Fig. 6. Hourly averaged Kp and f10.7 indices at 13:00 UTC were 1.7 and 114.3, respectively. The magnetic local time is approximately UTC + 2.5 h.

With IRI prior the maximum densities are slightly pronounced and the peak altitude remains below the UHF peak. With the zero mean prior both the profile shapes and peak densities clearly disagree with the UHF, again. For the ionosonde case the best agreement in general profile shape is again visible, even though the errors in peak altitudes and densities are in the same level with the IRI-based reconstructions.

3.4 Overflight IV

The COSMOS 2407 overflight starting at 21 November 2014 02:50 UTC (Fig. 7). Direction of the satellite track is from north to south. The relative phase difference curves in Fig. 8 indicate more small scale structure in ionosphere than in the previous measurements. The ionosonde measurements were collected at 02:56, 02:58, 03:02 and 03:04 UTC, as the data for 03:00 is missing. The measurements show a strong E-region at 100 km altitude. As the ionosonde measurements indicate that the electron density is not concentrated to one altitude, the maximum of the prior standard deviation is here set to the lower E-region peak of the ionosonde profile and the upper scale height is increased to 600 km to allow more variation also around the higher F-region peak. Otherwise the prior profiles are formed similarly to previous cases. The reconstruction and the EISCAT UHF measurement directions at (1) 02:57:40–02:58:50, (2) 02:59:15–03:00:30, (3) 03:00:50–03:02:05 and (4) 03:02:25–03:03:35 UTC are shown in top left

AMTD
8, 9823–9851, 2015

panel Fig. 8. Hourly averaged Kp and f10.7 indices at 03:00 UTC were 3.3 and 158.6, respectively. The magnetic local time is approximately UTC + 2.5 h.

With IRI prior an F-region is visible, although at wrong altitude, but the E-region peak is completely missing. The zero mean prior spreads electron density also to lower altitudes, but cannot distinguish the two peak structure. With ionosonde the shape of the reconstruction seems to be strongly dictated by the prior. Horizontal gradients in F-region peak density are rather well reproduced in the reconstruction, whereas the reconstructed E-region peak is almost unchanged in the profile comparisons, although the UHF radar shows significantly different peak density at each pointing direction. In the reconstruction on upper left panel of Fig. 8 a southward decrement in E-region density is visible between the receivers, where the information provided by the measurements is higher. Directly above the receivers information about the vertical profile is very poor and the reconstruction relies on the prior information. Hence the lower layer remains.

4 Conclusions

In this study the use of Bayesian statistical inversion with known prior distributions and with the inclusion of simultaneous ionosonde measurements for ionospheric tomography is validated. Most importantly we show that the prior distribution can be constructed based on the ionosonde measurements, which helps in constraining the otherwise poorly defined altitude profile shape of the tomographic reconstruction.

We demonstrate the applicability of the method with four satellite overflights measured with the TomoScand receiver network, and with EISCAT dynasonde measurements from the EISCAT Tromsø site. In comparisons we used International Reference Ionosphere 2007 and zero mean in building of the prior. The validation is made against simultaneous EISCAT UHF incoherent scatter radar measurements.

With IRI-2007 the biggest issue are the problems with the peak altitude. With zero mean it is the significant underestimation of the electron density. From both of the

AMTD
8, 9823–9851, 2015

reference schemes it can be seen that the measurements cannot provide enough information on the vertical gradients of the ionosphere. This information has to come from the prior distribution and needs to be accurate enough. The use of ionosonde in the building of the prior distribution outperforms the compared alternatives. The results show better agreement between the incoherent scatter radar measurements and the corresponding electron density profiles taken from the reconstruction. The reconstructions seem reasonable even further away from the ionosonde location. However, the electron density height profiles are dictated by the prior model, and could be biased further away from the ionosonde. Use of multiple ionosondes and altering the prior profile in horizontal direction would be straightforward within the method and highly recommended.

The results also indicate that when reliable prior information is provided, the required prior parameters can be predetermined and the method used without additional tuning. In the overflights I, II and III the changes in prior parameter values were done completely based on the current ionosonde measurements or IRI-2007 values. In Overflight IV also the shape of the prior standard deviation was changed, but the results indicate that this can also be based on the ionosonde measurements. This makes the operational stand-alone use feasible, at least for typical ionospheric conditions. With the lattice sizes in the reported scale and with a modern PC the required computations can be made in real-time.

As in the Bayesian inference we are presenting the information as probability distributions, we also have a straight access to the credible intervals. However, it is important to note that when interpreting the posterior distribution and credible intervals derived from it, they are highly dependent on the given prior distribution. Posterior credible intervals should thus be used with caution. If the prior is truly realistic, the posteriori credible interval can be highly informative.

As the ionosonde measurements provide relatively accurate measurements of the ionospheric electron density, it would be straightforward to use them also as direct measurements above the instrument location. However, the satellite overflight hits rarely at

AMTD
8, 9823–9851, 2015

the zenith of the ionosonde site and the electron densities measured by ionosonde and tomographic receiver can vary largely. When 2-D assumption (i.e. small gradients in longitude) is used, the ionosonde measurement error should reflect this discrepancy. Hence the information for the projected ionosonde measurement points cannot be modeled as accurately as they are in their actual location and the prior distribution provides substantially the same information. In the 3-D situation the situation will be different as all of the measurements will be modeled in their actual locations.

Acknowledgements. The work of L. Roininen has been funded by European Research Council (ERC Advanced Grant 267700 – InvProb). Ionospheric tomography measurements and analyzed data products used in this paper are freely available upon request from Finnish Meteorological Institute. Authors thank EISCAT staff, especially Jussi Markkanen, for kindly assisting in the EISCAT UHF radar experiments, and Yoshimasa Tanaka and Yasunobu Ogawa of NIPR for executing the EISCAT UHF radar experiments in March 2015. We also like to thank the EISCAT Scientific Association for providing the dynasonde data. EISCAT is an international association supported by research organisations in China (CRIRP), Finland (SA), Japan (NIPR and STEL), Norway (NFR), Sweden (VR), and the UK (NERC).

References

Andreeva, E. S.: Radio tomographic reconstruction of ionization dip in the plasma near the Earth, J. Exp. Theor. Phys. Lett., 52, 142–148, 1990. 9825

Austen, J. R., Franke, S. J., and Liu, C. H.: Ionospheric imaging using computerized tomography, Radio Sci., 3, 299–307, 1988. 9824

Bilitza, D. and Reinisch, B. W.: International Reference Ionosphere 2007: improvements and a new parameters, Adv. Space Res., 42, 599–609, 2008. 9827

Bust, G. S. and Mitchell, C. N.: History, current state, and future directions of ionospheric imaging, Rev. Geophys., 46, RG1003, doi:10.1029/2006RG000212, 2008. 9824

Chartier, A. T., Smith, N. D., Mitchell, C. N., Jackson, D. R., and Patilongo, P. J. C.: The use of ionosondes in GPS ionospheric tomography at low latitudes, J. Geophys. Res., 117, A10326, doi:10.1029/2012JA018054, 2012. 9826

Davies, K.: Ionospheric Radio IEE Electromagn. Waves ser., IET, London, 1990. 9828

AMTD

8, 9823–9851, 2015

Kaipio, J. and Somersalo, E.: Statistical and Computational Inverse Problems, Applied Mathematical Sciences, Springer, New York, 2005. 9829

Kersley, L., Heaton, J. A. T., Pryse, S. E., and Raymund, T. D.: Experimental ionospheric tomography with ionosonde input and EISCAT verification, Ann. Geophys., 11, 1064–1074, 1993, http://www.ann-geophys.net/11/1064/1993/. 9826

Markkanen, M., Lehtinen, M., Nygren, T., Pirttilä, J., Helenius, P., Vilenius, E., Tereshchenko, E. D., and Khudukon, B. Z.: Bayesian approach to satellite radiotomography with applications in the Scandinavian sector, Ann. Geophys., 13, 1277–1287, 1995, http://www.ann-geophys.net/13/1277/1995/. 9825, 9828

Norberg, J., Roininen, L., Vierinen, J., Amm, O., McKay-Bukowski, D., and Lehtinen, M. S.: Ionospheric tomography in Bayesian framework with Gaussian Markov random field priors, Radio Sci., 50, 138–152, doi:10.1002/2014RS005431, 2015. 9825, 9826, 9830

Vierinen, J., Norberg, J., Lehtinen, M. S., Amm, O., Roininen, L., Väänänen, A., and McKay-Bukowski, D.: Software defined beacon satellite receiver software for ionospheric tomography, Radio Sci., 49, 1141–1152, doi:10.1002/2014RS005434, 2014. 9827

Zabotin, N. A., Wright, J. W., and Zhbankov, G. A.: NeXtYZ: three-dimensional electron density inversion for dynasonde ionograms, Radio Sci., 41, RS6S32, doi:10.1029/2005RS003352, 2006. 9831

AMTD
8, 9823–9851, 2015

Table 1. Errors of tomographic profiles compared with EISCAT UHF scans in Overflight I.

	Relative mean error of peak density (%)	Mean error of peak altitude (km)
Ionosonde	5	41
IRI	27	55
Zero	52	74

AMTD
8, 9823–9851, 2015

Table 2. Errors of tomographic profiles compared with EISCAT UHF scans in Overflight II.

	Relative mean error of peak density (%)	Mean error of peak altitude (km)
Ionosonde	5	17
IRI	6	58
Zero	54	15

AMTD
8, 9823–9851, 2015

Table 3. Errors of tomographic profiles compared with EISCAT UHF scans in Overflight III.

	Relative mean error of peak density (%)	Mean error of peak altitude (km)
Ionosonde	4	33
IRI	6	31
Zero	60	33

AMTD
8, 9823–9851, 2015

Table 4. Errors of tomographic profiles compared with EISCAT UHF scans in Overflight IV.

	Relative mean error of peak density (%)	Mean error of peak altitude (km)
Ionosonde	5	40
IRI	12	84
Zero	61	50

AMTD
8, 9823–9851, 2015

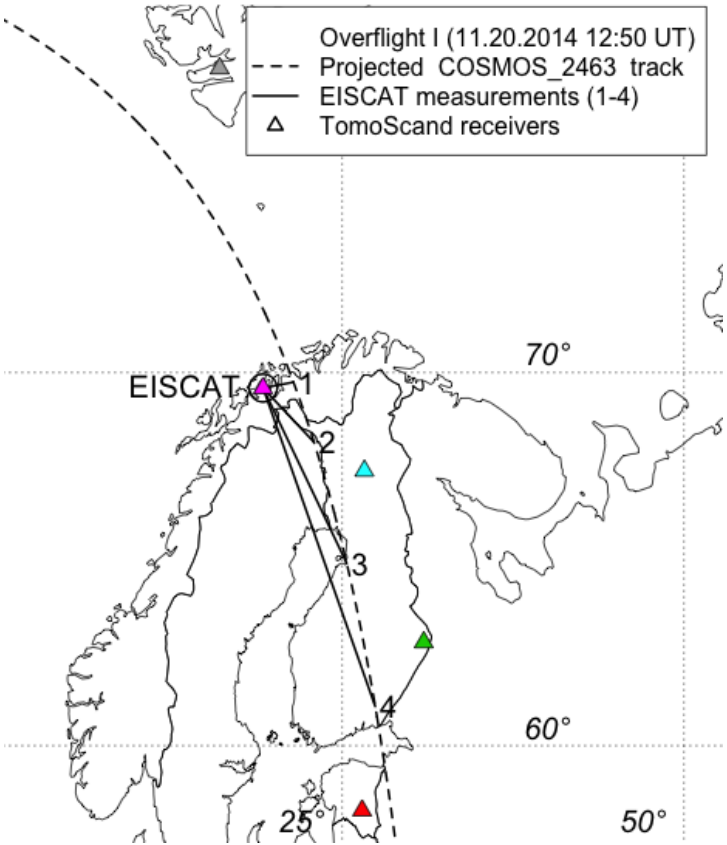

Figure 1. TomoScand receiver network and the satellite overflight ground track with four EISCAT UHF scan paths.

AMTD
8, 9823–9851, 2015

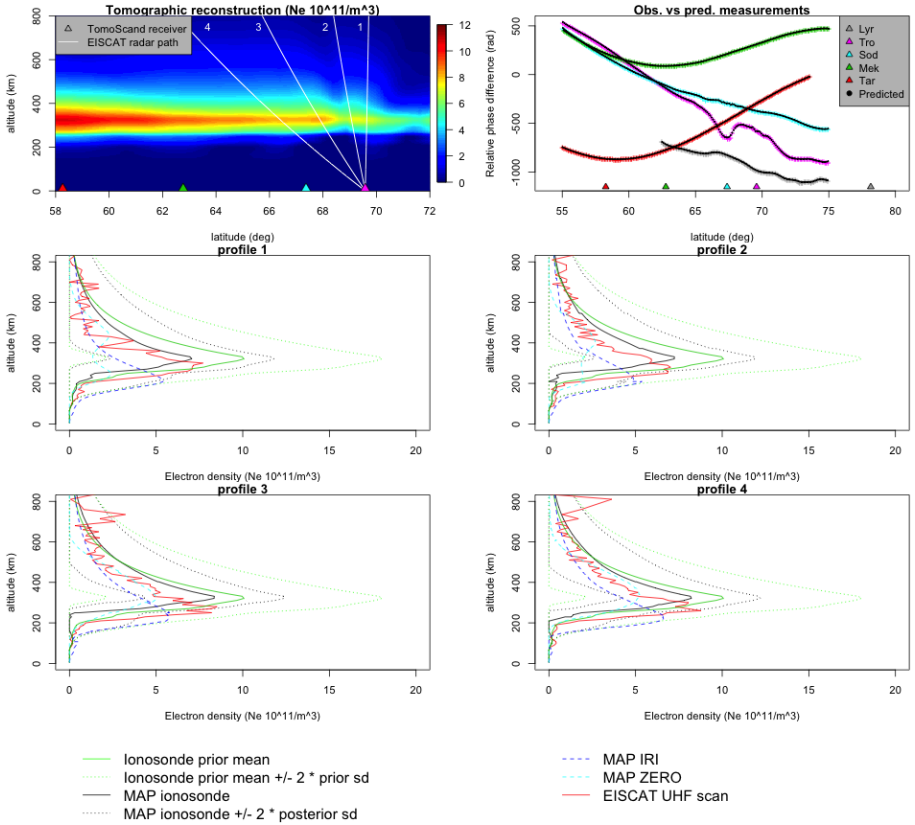

Figure 2. Reconstruction, phase curves and profile comparisons for Overflight I starting at 20 November 2014 12:50 UTC.

AMTD
8, 9823–9851, 2015

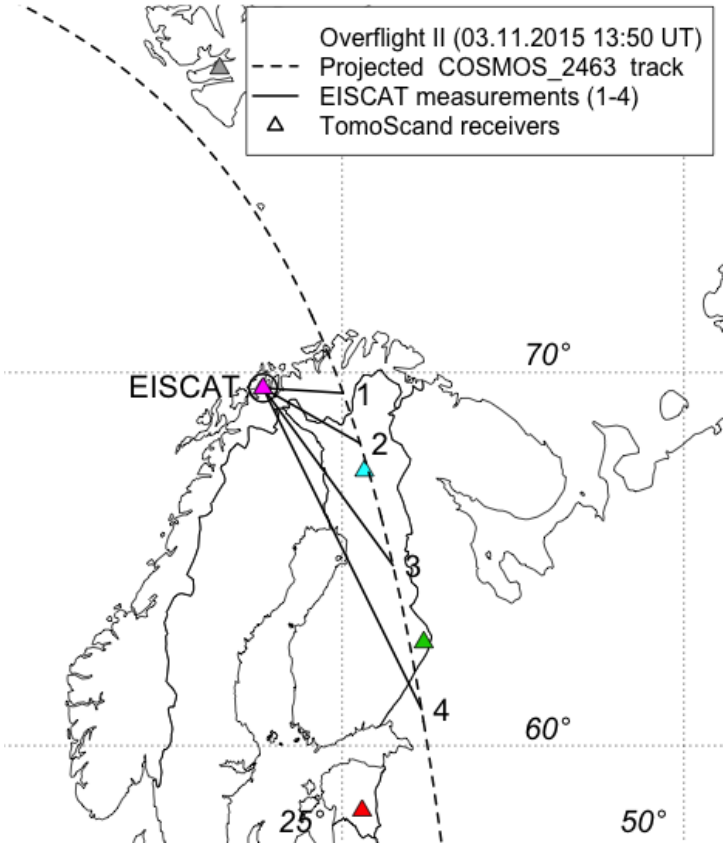

Figure 3. TomoScand receiver network and the satellite overflight ground track with four EISCAT UHF scan paths.

AMTD
8, 9823–9851, 2015

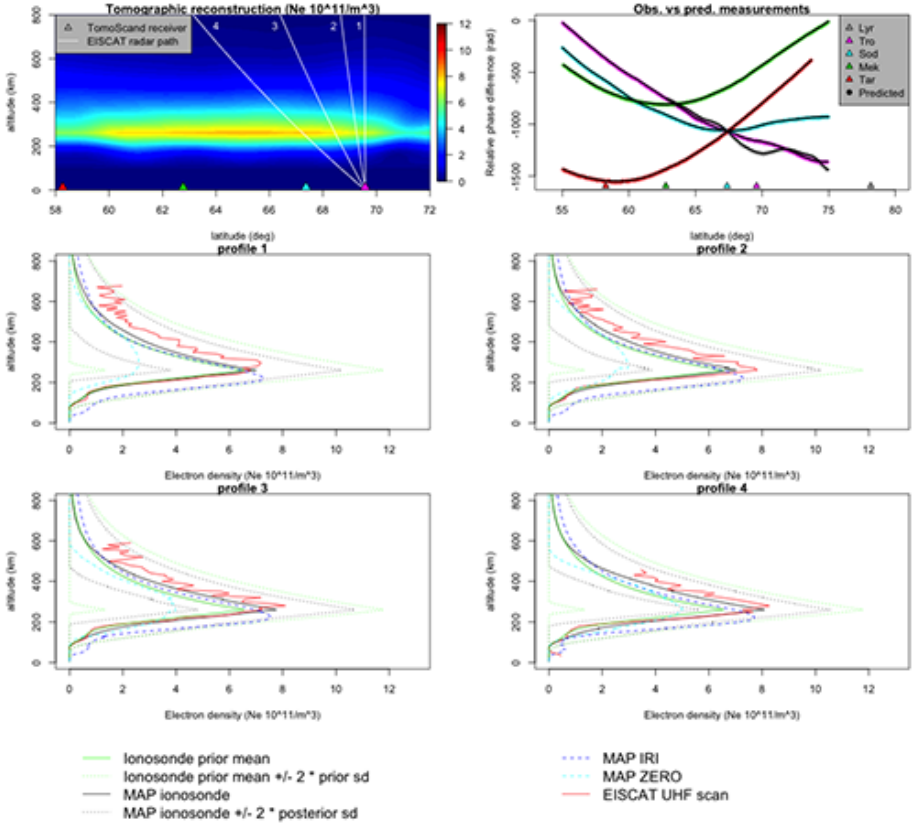

Figure 4. Reconstruction, phase curves and profile comparisons for Overflight II starting at 3 November 2015 13:50 UTC.

AMTD
8, 9823–9851, 2015

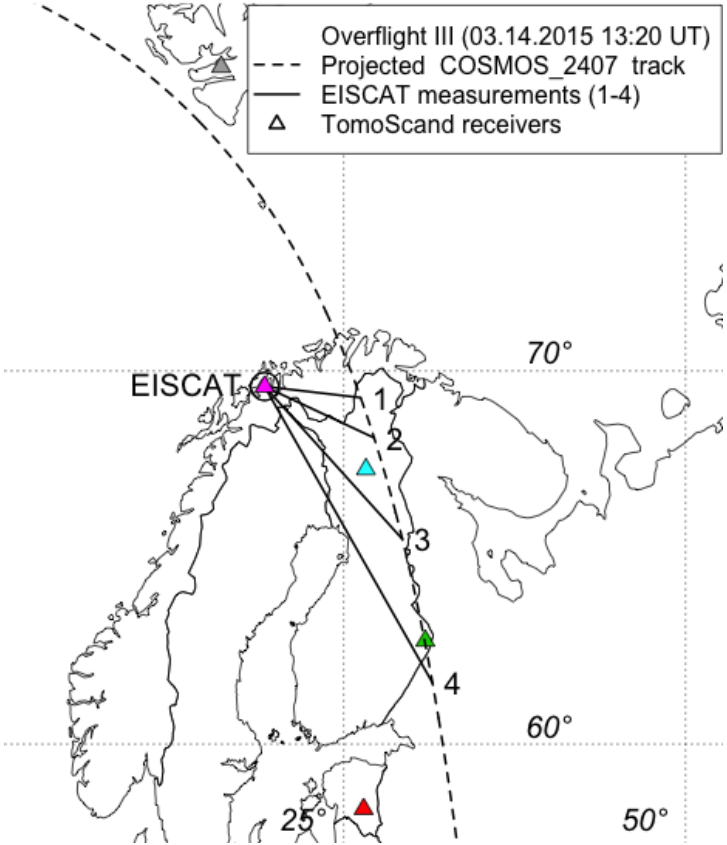

Figure 5. TomoScand receiver network and the satellite overflight ground track with four EISCAT UHF scan paths.

AMTD
8, 9823–9851, 2015

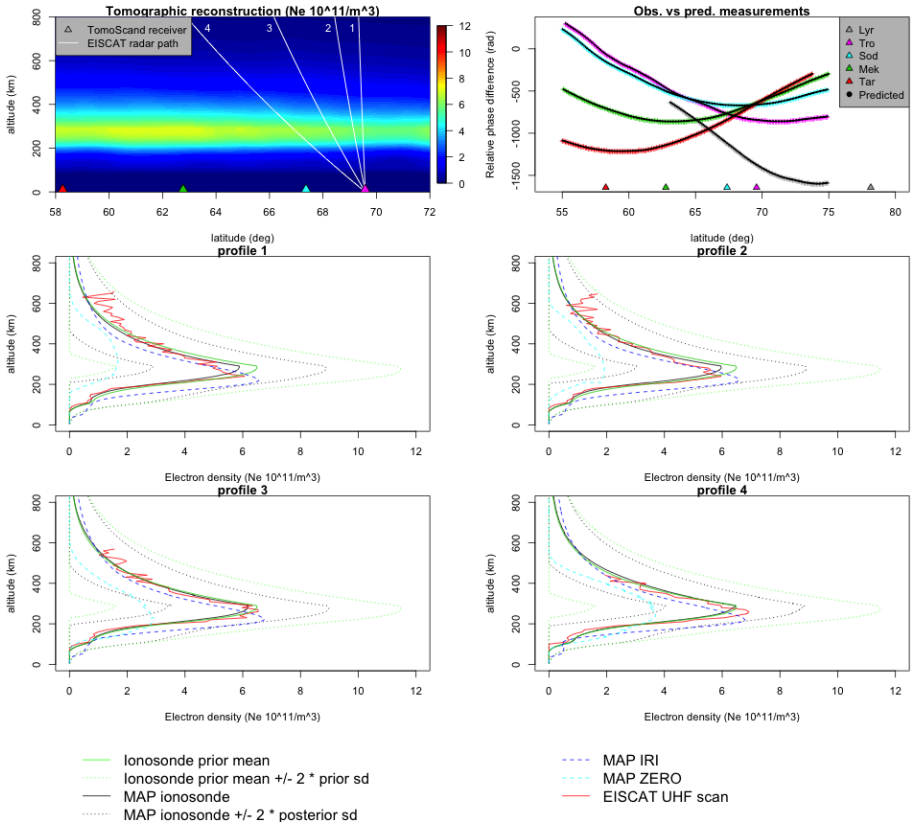

Figure 6. Reconstruction, phase curves and profile comparisons for Overflight III starting at 14 November 2015 13:20 UTC.

AMTD
8, 9823–9851, 2015

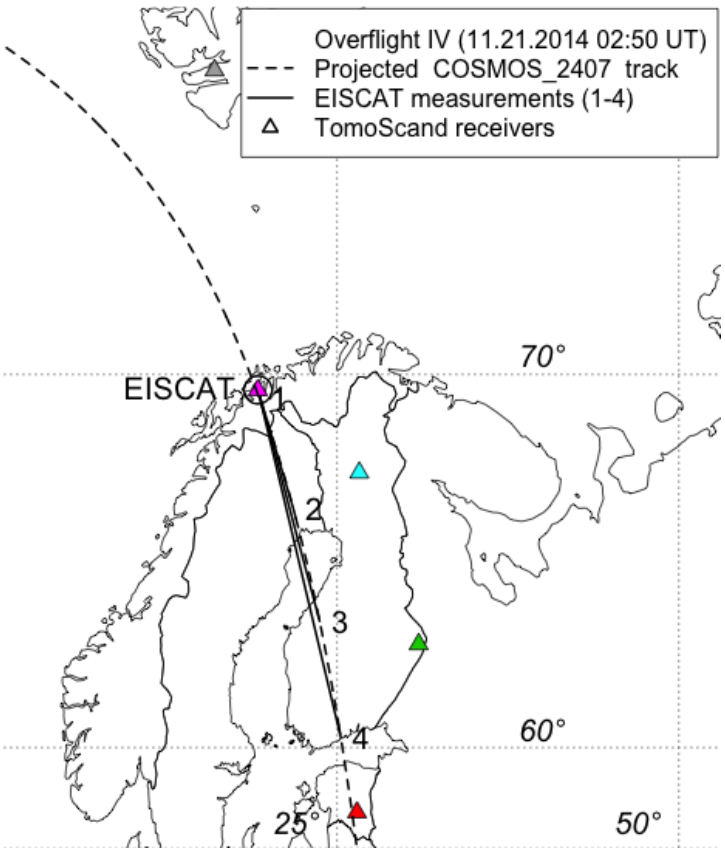

Figure 7. TomoScand receiver network and the satellite overflight ground track with four EISCAT UHF scan paths.

AMTD
8, 9823–9851, 2015

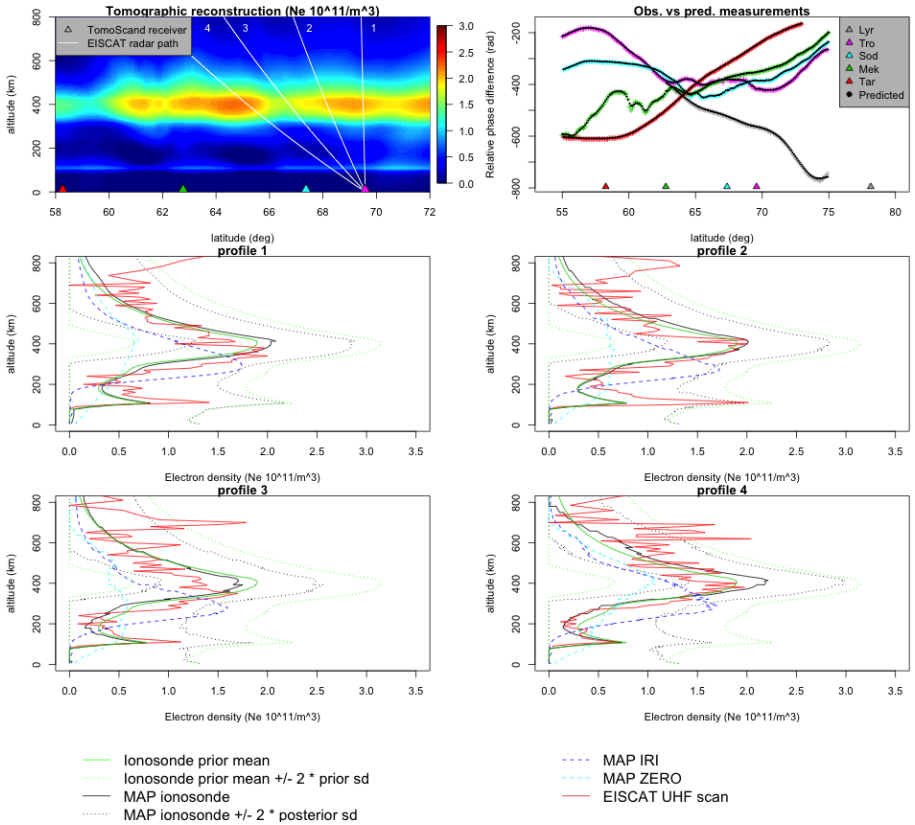

Figure 8. Reconstruction, phase curves and profile comparisons for Overflight IV starting at 20 November 2014 02:50 UTC.

AMTD
8, 9823–9851, 2015